JPET Fast Forward. Published on November 8, 2021 as DOI: 10.1124/jpet.121.000852
This article has not been copyedited and formatted. The final version may differ from this version.

Thiabendazole inhibits glioblastoma cell proliferation and invasion targeting MCM2

Yaotian Hu[1], Wenjing Zhou[1], Zhiyi Xue[1], Xuemeng Liu[1], Zichao Feng[1], Yulin Zhang[1], Xiaofei Liu[1], Wenjie Li[1], Qing Zhang[1], Anjing Chen[1], Bin Huang[1] and Jian Wang[1, 2]

[1]Department of Neurosurgery, Qilu Hospital and Institute of Brain and Brain-Inspired Science, Cheeloo College of Medicine, Shandong University, Jinan, China

Shandong Key Laboratory of Brain Function Remodeling, Jinan, China

[2]Department of Biomedicine, University of Bergen, Jonas Lies vei 91, 5009 Bergen, Norway

JPET Fast Forward. Published on November 8, 2021 as DOI: 10.1124/jpet.121.000852
This article has not been copyedited and formatted. The final version may differ from this version.

a) Running title: Thiabendazole repurposing in glioblastoma cells and its function

b) Correspondence to:

Jian Wang

Address: Department of Neurosurgery, Qilu Hospital of Shandong University and Brain Science Research Institute, Shandong University, Jinan, China

No.107 Wenhua Xi Road, Jinan 250012, P.R. China

Telephone: +86-531-82169428

Fax numbers: +86-531-82166615

E-mail: jian.wang@uib.no

c) The number of text pages: 35

The number of figures: 6

The number of references: 36

The number of words in the *Abstract*: 226

The number of words in the *Introduction*: 495

The number of words in the *Discussion*: 755

d) Nonstandard Abbreviations: MCM2, mini-chromosome maintenance protein 2; TBZ, thiabendazole

e) Recommended Section Assignment: Neuropharmacology

JPET Fast Forward. Published on November 8, 2021 as DOI: 10.1124/jpet.121.000852
This article has not been copyedited and formatted. The final version may differ from this version.

Abstract

Thiabendazole (TBZ), approved by the U.S. Food and Drug Administration (FDA) for human oral use, elicits a potential anti-cancer activity on cancer cells *in vitro* and in animal models. Here, we evaluated the efficacy of TBZ in the treatment of human glioblastoma multiforme (GBM). TBZ reduced the viability of GBM cells (P3, U251, LN229, A172, and U118MG) relative to controls in a dose- and time-dependent manner. However, normal human astrocytes (NHA) exhibited a greater IC50 than tumor cells lines and were thus, more resistant to its cytotoxic effects. EdU positive cells and the number of colonies formed was decreased in TBZ-treated cells (at 150 μM, $P < 0.05$ and at 150 μM, $P < 0.001$, respectively). This decrease in proliferation was associated with a G2/M arrest as assessed with flow cytometry, and the downregulation of G2/M check point proteins. In addition, TBZ suppressed GBM cell invasion. Analysis of RNA sequencing data comparing TBZ treated cells with controls yielded a group of differentially expressed genes, the functions of which were associated with the cell cycle and DNA replication. The most significantly downregulated gene in TBZ-treated cells was mini-chromosome maintenance protein 2 (MCM2). SiRNA knockdown of MCM2 inhibited proliferation, causing a G2/M arrest in GBM cell lines and suppressed invasion. Taken together, our results demonstrated that TBZ inhibited proliferation and invasion in GBM cells through targeting of MCM2.

Keywords: TBZ, GBM, G2/M arrest, invasion, MCM2

JPET Fast Forward. Published on November 8, 2021 as DOI: 10.1124/jpet.121.000852
This article has not been copyedited and formatted. The final version may differ from this version.

Significance Statement

TBZ inhibits the proliferation and invasion of glioblastoma cells by downregulating the expression of MCM2. These results support the repurposing of TBZ as a possible therapeutic drug in the treatment of GBM.

JPET Fast Forward. Published on November 8, 2021 as DOI: 10.1124/jpet.121.000852
This article has not been copyedited and formatted. The final version may differ from this version.

Introduction

Glioblastoma multiforme (GBM) is the most common and malignant primary brain tumor in human adults with only 14.6 months of median survival after primary diagnosis (Darlix et al., 2017), despite a standard therapeutic regimen consisting of surgery, radiotherapy and chemotherapy (Ostrom et al., 2020). The current chemotherapy used is often temozolomide, an oral DNA alkylating agent, which in combination with radiotherapy following surgery has increased patient survival from 12.1 to 14.6 months (Stupp et al., 2005). However, at least 50% of GBM patients do not respond (Lee, 2016). Several biological properties of GBM render the disease resistant to treatment. First, GBM cells filtrate the peripheral normal brain tissue, making complete removal of the tumor with surgery impossible (Bell and Karnosh, 1949; Shergalis et al., 2018). Second, most chemotherapeutic molecules insufficiently permeate the brain due to the blood-brain barrier (BBB) (Shergalis et al., 2018). Third, targeting of key molecular pathways is ineffective because of the high cellular and genetic heterogeneity within GBM (Brennan et al., 2013). Thus, novel effective drugs and therapeutic targets are urgently needed for GBM treatment.

Drug repurposing has become a widely accepted strategy in oncology to identify new therapies. Drugs already known to be safe in humans accelerate the initiation of clinical trials needed especially in the case of cancers with few treatment options. For instance, flubendazole and mebendazole are benzimidazole carbamate family compounds approved for use as anthelminthics in humans and have been studied for their anticancer properties against diverse cancers including human glioma.

JPET Fast Forward. Published on November 8, 2021 as DOI: 10.1124/jpet.121.000852
This article has not been copyedited and formatted. The final version may differ from this version.

Flubendazole has been shown to inhibit glioma proliferation and tumorigenesis. Mebendazole was shown to be cytotoxic to glioma and significantly prolonged mean survival in syngeneic and xenograft orthotopic animal glioma models (Bai et al., 2011). In a phase 1 clinical trial, mebendazole demonstrated long-term safety and acceptable toxicity at doses of up to 200 mg/kg (Gallia et al., 2021). Another benzimidazole, thiabendazole (TBZ; tiabendazole; 2-(thiazol-4-yl) benzimidazole), has been used to treat gut parasites in humans for over 50 years (Campbell and Cuckler, 1969; Whalen et al., 1971). TBZ inhibits blastocysts, candida albicans, penicillium and psoriasis, and prevents the formation of aflatoxin in plant feed, but it does not affect carcinogenesis and fertility in animals (Gosselin et al., 1984). A previous study demonstrated that TBZ reduced the growth of human fibrosarcoma (Cha et al., 2012). Therefore, as a non-toxic member of the family of benzimidazole compounds, TBZ has gained interest for its potential as an anticancer therapy in humans.

In this study, we examined the anticancer effects of TBZ and investigated its potential molecular mechanisms in GBM cells *in vitro* and *in vivo*. We demonstrated that TBZ induces G2/M arrest in GBM cells and inhibits invasion. We performed RNA sequencing on the tumor cells treated with TBZ to identify differentially expressed genes and found mini-chromosome maintenance protein 2 (MCM2) to be a key transcriptional factor downregulated by TBZ, showing the MCM2 as a molecular target of TBZ. Finally, we determined that TBZ inhibits GBM cells growth *in vivo*.

JPET Fast Forward. Published on November 8, 2021 as DOI: 10.1124/jpet.121.000852
This article has not been copyedited and formatted. The final version may differ from this version.

Materials and Methods

Ethics statement

Nude mice (age, 4 weeks; weight, 14 to 17 g) were purchased from the Nanjing Biomedical Research Institute of Nanjing University (Nanjing, China) and maintained in the animal facility of Qilu Hospital, Shandong University under pathogen-free conditions. Ethical approval was granted by the Ethics Committee/Laboratory Animal Research Center protocols of Qilu Hospital, Shandong University (Jinan, China).

Cell lines and cultures

GBM cell lines, U251, LN229, A172, U118MG, and Normal human astrocytes (NHA) were purchase from by the Chinese Academy of Sciences Cell Bank (Shanghai, China) and authenticated by short tandem repeat (STR) profiling. The cells are anchorage-dependent cells in the absence of any stress. Complete medium for NHA, U251, LN229, A172 and U118MG is made up of the following reagents: Dulbecco's modified Eagle's medium (DMEM; Thermo Fisher Scientific; Waltham, MA, USA), 10% fetal bovine serum (FBS; Thermo Fisher Scientific), streptomycin (100 U/mL) and penicillin (100 U/mL). The cells were culture in a humidified incubator (HERAcell 204i, ThermoFisher Scientific) at 37°C, 5% CO_2.

The P3 cells used in the study were derived from a primary human GBM cells and were cultured in Neurobasal Medium (NBM; 21103-049, ThermoFisher Scientific) supplemented with 2% B27 (cat#A3653401, ThermoFisher Scientific), 1% L-glutamine (BE17-605E, BioNordika; Oslo, Norway), 1% penicillin/streptomycin (17-603E, BioNordika), 20 ng/mL EGF (AF-100-15, Peprotech; Rocky Hill, NJ, USA) and

20 ng/mL bFGF (100-18B, Peprotech) in a humidified incubator at 37°C , 5% CO_2. The cells were sub-cultured every 3 days at a sub-culture ratio of 1:3. A PCR-based assay was used to detect mycoplasma contamination.

Antibodies and reagents

Mini-chromosome maintenance complex component 2 (MCM2, western-blotting dilution 1:1000), cyclin dependent kinase 1 (CDK1, western-blotting dilution 1:1000), cyclin B1 (western-blotting dilution 1:1000), N-cadherin (western-blotting dilution 1:1000), zinc finger E-box binding homeobox 1 (ZEB1, western-blotting dilution 1:1000) and glyceraldehyde-3-phosphate dehydrogenase (GAPDH, western-blotting dilution 1:1000) were purchased from Cell Signaling Technology (Danvers, MA, USA).

Actin beta (ACTB, β-actin, western-blotting dilution 1:1000), proliferating cell nuclear antigen (PCNA, western-blotting dilution 1:1000), cyclin B2 (western-blotting dilution 1:1000) and Ki67 (Immunohistochemistry dilution 1:200) were purchased from Abcam (Cambridge, UK).

Mini-chromosome maintenance complex component 5 (MCM5, western-blotting dilution 1:1000), matrix metalloproteinase 2 (MMP2, western-blotting dilution 1:1000) were purchased from Proteintech (Rosemont, IL, USA).

Ubiquitin like with PHD and ring finger domains 1 (UHRF1, western-blotting dilution 1:1000) was purchased from Santa Cruz (Dallas, TX, USA).

HRP-labeled goat anti-rabbit secondary antibodies were provided by Zhongshan Golden Bridge Bio-technology (Beijing, China). Proteins on western blots were measured with enhanced chemiluminescence (Millipore; Burlington, MA, USA). The

JPET Fast Forward. Published on November 8, 2021 as DOI: 10.1124/jpet.121.000852
This article has not been copyedited and formatted. The final version may differ from this version.

PI/RNase staining buffer kit was provided from BD Pharmingen (San Diego, CA, USA).

TBZ (45684, Sigma-Aldrich; St. Louis, MO, USA) was dissolved in dimethyl sulfoxide (DMSO; D2650, Sigma-Aldrich) at a concentration of 100 mM, stored at -20℃, and diluted to working concentrations in culture medium when needed. The diluted TBZ was used within 1 month.

The 96 well 3D spheroid cell reagent kit (3500-096-K, Cultrex) was purchased from Trevigen (Gaithersburg, MD, USA).

Cell viability assay

Cell Counting Kit-8 assay (CCK-8; Dojindo, Kumamoto, Japan) was used to assess cell viability. 4×10^3 of GBM cells were seeded into each well of 96-well plates (Corning; Corning, NY, USA) and cultured in a humidified incubator at 37°C, 5% CO2. After 24 h, the medium was replaced with 100 μL of fresh culture medium containing different concentrations of TBZ or vehicle control (DMSO). At 24 h, 48 h, 72 h, and 96 h after dosing, GBM cells were incubated with 10 μL of CCK-8 reagent in 100 μL of serum-free DMEM at 37°C for 1 h and an EnSight Multimode Plate Reader (PerkinElmer; Singapore) was used to measure the absorbance at 450 nm. Cell viability of GBM cells transfected with MCM2 siRNA and overexpression constructs was also assessed with the CCK-8 assay.

Cell proliferation assay

1×10^4 of GBM cells were seeded into each well of 24-well plates (Corning) and cultured in a humidified incubator at 37°C, 5% CO2. 5-ethynyl-2'-deoxyuridine (EdU) was diluted 1:1000 in DMEM complete medium, and GBM cells were treated with the

JPET Fast Forward. Published on November 8, 2021 as DOI: 10.1124/jpet.121.000852
This article has not been copyedited and formatted. The final version may differ from this version.

EdU mixed medium for 1 h. EdU was detected through a catalyzed reaction between EdU and Apollo fluorescent dyes provided in the EdU incorporation assay (C103103, Ribobio; Guangzhou, China). Apollo dying solution was prepared as follows: 4,690 μL of distilled water, 250 μL of Apollo® reaction buffer, 50 μL of Apollo® catalyst solution, 15 μL of Apollo® fluorescent dye solution, and 44 mg of Apollo® buffer additive. 250 μL of Apollo dying solution was added to each well. Nuclei were counterstained with DAPI. EdU-positive cells were counted under fluorescence microscopy (Leica; Solms, Germany).

Colony formation assay

U251 and P3 cells were counted, the cell density was diluted to 500 cells/mL, and 2 mL of the cell suspension was added to each well of a 6-well plate (Corning). The drug concentrations used were the following: 0 μM (DMSO), 150 μM and 300 μM, following 7 days culture. The medium was then replaced with fresh medium and cells were continued culture for an additional 7 days. The culture medium was discarded, each well of the 6-well plate was rinsed with 500 μL PBS (3x), and the cells were fixed with 4% paraformaldehyde for 15 min. Each well of the 6-well plate was rinsed with 500 μL PBS (3x) and cells were stained for 30 min with crystal violet. The wells were slowly rinsed with double distilled water. Clones were counted after air drying the wells. Clones were counted if the number of cells was > 50.

Protein lysates and Western blotting

GBM cells were lysed with RIPA Lysis Buffer (Beyotime; Shanghai, China) supplemented with phenylmethanesulfonyl fluoride (PMSF, Beyotime) for 30 minutes

after 48 h treatment. Lysates were centrifuged at 13,000 rpm/min for 20 min (Centrifuge 5804R, Thermo Fisher Scientific; Waltham, MA), and protein concentrations were assessed with the BCA assay according to the manufacturer's instructions (Beyotime, China).

The PAGE Gel Fast Preparation Kit (PG112, Epizyme, Shanghai, China, 4℃ storage) was used to prepare 1.5 mm thick, 10% gels with 15 wells according to the manufacturer's instructions.

Cell lysates (20 μg protein) were subjected to western blot analysis, according to previously described protocols (Kong et al., 2019). Membranes were incubated with primary antibody at 4℃ overnight followed by incubation with appropriate secondary antibodies (1:2000) for 1 h at room temperature. Chemiluminescent signals were imaged using the Chemiluminescence Imager (Bio-Rad; Hercules, CA, USA) according to the manufacturer's protocol. Band density was quantified with ImageJ software and normalized to GAPDH or β-actin. All experiments were repeated three times.

Cell cycle

U251 and P3 cells were diluted to 4×10^5 cells /mL and 2 mL of the cell suspension was seeded into each well of a 6-well plate, and cultured overnight. TBZ were added to cells at the following concentrations: 0 μM (DMSO), 150 μM and 300 μM. After 2 days, cells were rinsed and harvested at 4000 rpm/min for 5 min, and gently fixed in fresh 300 μL PBS and 700 μL 75% ethanol. Cells were incubated at 4℃ overnight, harvested at 4,000 rpm/min for 5 min, rinsed with PBS at 4,000 rpm/min for 5 min. The cell

pellets were stained with propidium iodide (PI, BD Biosciences; San Jose, CA, USA) dye solution for 20 min and then followed by flow cytometry for cell cycle analysis. In gate P1, the linear relationship was set for F2L-A and F2L-H. Gate P2 is looped to select diploid and tetraploid cells, and 10,000 events are collected under P2 conditions. Data was exported, and Modifit 2.0 software was used to determine the cell cycle distribution. GBM cells transfected with MCM2 siRNA and MCM2 overexpression constructs were similarly processed to obtain cell cycle parameters.

Trans-well invasion assay

U251 and P3 cells were diluted to 4×10^5 cells /mL, and 2 mL of cell suspension was seeded into each well of a 6-well plate. The cells were incubated under different conditions for 48 h. Trans-well migration plates with 8 μm pore size (Corning; Sigma-Aldrich) were coated with Matrigel (Becton-Dickinson; Bedford, MA, USA) for 4 h. 20,000 cells in 100 μL DMEM without FBS were seeded into the upper chamber of a trans-well apparatus and 600 μL medium containing 10% FBS was added to the lower chamber. After 24 h incubation at 37°C, cells remaining were removed from the top side of the insert with a cotton swab and the migrated cells were fixed with 4% paraformaldehyde for 15 min, rinsed twice with PBS and stained with crystal violet for 30 min. The dye was removed, and cells were rinsed with double distilled water. Images from 3 random views under a light microscope were acquired and used to count migrated cells.

Cell invasion in 3D culture

3,000 cells were seeded into each well of 3D Culture Qualified 96-well spheroid

formation plates (Trevigen) with 100 μL of medium and cultured at 37°C, 5% CO_2 for 72 h in a humidified incubator. After 72 h, U251 and P3 cells formed tumor spheroids. Plates were placed on ice for 15 min, and 50 μL of invasion matrix (Trevigen, 3500-096-03) was added to each well in the plates. Plates were centrifuged at 300×g at 4°C for 5 min and incubated at 37°C for 1 h. Conditioned medium (100 μL) with different concentrations of TBZ was added to each well of the plates. P3 tumor spheroids were incubated for 3 days and U251 tumor spheroids were incubated for 10 days. Images of the spheroids were captured every 24 h under bright field microscopy with a 4× objective. The 192-hour images of U251 and the 48-hour image of P3 were analyzed with the software ImageJ. GBM cells after transfection with MCM2 siRNA or MCM2 overexpression constructs were also assessed in 3D invasion culture as described above.

RNA-seq and bioinformatics analysis

The RNA-Seq libraries were prepared using the Illumina TruSeq™ RNA sample preparation Kit (Illumina, San Diego, CA), and sequenced through paired-end (150 base paired-end reads) sequencing performed on the Illumina NovaSeq 6000 platform. Raw data was then quality filtered to generate “clean reads” for further analysis. The “clean reads” were then aligned to the human genome reference (hg19) using STAR software and the reference-based assembly of transcripts was conducted using HISAT2. We used picard to compare the results and to remove redundancy, and used Sentieon software to detect single nucleotide variations (SNVs) and InDels. All previously identified SNVs and InDels were determined by using the dbsnp database. Gene expression values were expressed as reads per kilobase of exon per million fragments

mapped (FPKM) using kallisto software. To identify true differentially expressed genes (DEGs), the false discovery rate (FDR) was used for the rectification of the p-values. The DEGs (P-value ≤ 0.05, |Log2FC|≥1) were subjected to enrichment analyses of GO and KEGG pathways. Protein-to-protein interaction network analyses of DEGs was performed using the STRING database and the protein-protein interaction networks were visualized with Cytoscape software.

RNA interference

GenePharma (Shanghai, China) used BLAST (www.ncbi.nlm.nih.gov/BLAST/) to select an appropriate target sequence and synthesized siRNAs. Interfering RNA sequences (siRNA) targeting human MCM2 (Gene Pharma Gene; Shanghai, China) were transfected into cells with Lipofectamine 2000 reagent (Thermo Fisher Scientific) according to the manufacturer's protocol. After 4 h, RNA expressing fluorescence was used to detect transfection efficiency. Western blot was used to determine the knockdown efficiency 48 h after transfection. SiRNA sequences used were the following: Negative control (sense 5'-UUC UCC GAA CGU GUC ACG UTT-3', antisense 5'-ACG UGA CAC GUU CGG AGA ATT-3'), MCM2-Homo-799 (sense 5'-GUG GUG AAC UAU GAG GAC UTT-3', antisense 5'-AGU CCU CAU AGU UCA CCA CTT-3'), MCM2-Homo-1211 (sense 5'-CCA UCU AUC AGA ACU ACC ATT-3', antisense 5'-UGG UAG UUC UGA UAG AUG GTT-3'), MCM2-Homo-1355 (sense 5'-GCA UCU AUC ACA ACU ATT-3', antisense 5'-UAG UUG UUG UGA UAG AUG CTT-3').

Lentiviral transduction

JPET Fast Forward. Published on November 8, 2021 as DOI: 10.1124/jpet.121.000852
This article has not been copyedited and formatted. The final version may differ from this version.

Lentiviral vectors expressing human mRNA targeting MCM2 (GenePharma, Shanghai) or scrambled-control (negative control) were used to generate stable cell clones overexpressing MCM2 or a nonspecific RNA as the control. Transfected clones were selected in 1 mg/mL of puromycin (Selleckchem; Houston, TX, USA) for 2 weeks. Western blot analysis was used to evaluate the transduction efficiency.

Orthotopic xnograft model

P3 cells expressing luciferase-GFP (X×10X; OBiO Technology; Shanghai, China) were implanted into the brains of nude mice. After 7 days, tumor was determined using bioluminescence imaging (PerkinElmer IVIS Spectrum; Waltham, MA, USA), and the mice were divided into the following 2 groups: control, n = 5; TBZ, n = 5. Mice were intraperitoneally injected with diluted DMSO alone (control) and TBZ (50 mg/kg/day) every day. Tumor volume was monitored using the bioluminescence imaging every week for 3 weeks, and the weight of each mouse was recorded every week for 4 weeks. Tumor bearing nude mice were treated until severe symptoms or death appeared imminent: the body weight had decreased > 10% and mice were unable to return upright after being pushed down. Survival (in days) was determined as the number of days starting from implantation (day 1) to death. Mice were euthanized at the end of the experiment. Excised tumor tissue was snap frozen in liquid nitrogen or formalin-fixed for further analysis.

Liquid chromatography-tandem mass spectrometry analysis

The nude mice were separated into TBZ-treated group (intraperitoneal injection, 3 mice) and control group (3 mice). Two hours after the injection, the mice were

JPET Fast Forward. Published on November 8, 2021 as DOI: 10.1124/jpet.121.000852
This article has not been copyedited and formatted. The final version may differ from this version.

anesthetized with chloral hydrate solution (Qilu hospital, China). PBS was perfused through the heart. The mice were sacrificed by CO_2 inhalation and the brain samples were collected and stored at -80°C. The TBZ and the brain samples were further analyzed by liquid chromatography-tandem mass spectrometry to examine the distribution of TBZ within the brain tissue. In brief, the tissue samples were weighed and appropriate amounts of methanol (chromatographically pure; Thermo Fisher, USA) and zirconia grinding beads were added (Servicebio, Wuhan, China). The samples were ground for 5 min after vortexing for 10 min, and then centrifuged at 15000 RPM for 10 min (centrifuge: D3024R, Dragonlab, Beijing, China). The supernatant was collected and diluted for the analysis on the UltiMate 3000 RS (ThermoFisher Scientific, USA) and TSQ Quantum (ThermoFisher Scientific, USA) instruments.

Plotting and statistical analysis

At least three times for each assay was independently conducted. All analyses were performed using GraphPad Prism 8.02 software (San Diego, CA, USA). Data were reported as the mean ± SD. The statistical significance of data was evaluated using a Student's t-test and the following p-values: $*P < 0.05$; $**P < 0.01$; $***P < 0.001$ were considered to be indicated as significant differences.

Results

Thiabendazole induces G2/M arrest in GBM cells

To determine whether TBZ is cytotoxic to GBM, we first exposed GBM cell lines and NHA to TBZ *in vitro*. The viability of all cells tested including P3, U251, LN229,

A172, U118MG and NHA, decreased in a dose-dependent manner with increasing concentrations of TBZ (Figure 1A). The IC50 of NHA was at least 100 μM greater than for all other cell lines indicating TBZ might be selective for tumor cells at certain concentrations (Figure 1B). In the functional experiments, we then chose P3, representing a primary GBM cell line and U251, representing one of most common GBM laboratory cell lines. In the colony forming assay, colony numbers were decreased by ~ 50% for P3 and U251 cells with 150 μM TBZ, and decreased by 90% for P3 and 75% for U251 with 300 μM TBZ (Supp. Fig. 1A and 1B). Finally, the viability of P3 and U251 cells under treatment with different TBZ concentrations was less at 96 h compared with 48 h (Figure 1C). These results indicated that TBZ potently reduced viability of GBM cells in a dose- and time-dependent manner.

Cell proliferation and cell cycle parameters were also examined in P3 and U251 cells under TBZ treatment. In P3 cells, EdU incorporation was reduced by 70% with 150 μM TBZ and 90% with 300 μM TBZ. In U251 cell lines, EdU incorporation was reduced by 40% with 150 μM TBZ and by ~ 70% with 300 μM TBZ. The EdU reduction in both P3 and U251 cell lines occurred in a dose-dependent manner with increasing TBZ concentrations (0 μM, 150 μM, and 300 μM) at 48 h (Figure 1D and Supp. Fig. 1C). Cell cycle analysis furthermore demonstrated that the percentage of GBM cells accumulated in G2/M increased under TBZ treatment in a dose-dependent manner (Figure 1E and Supp. Fig. 1D). Finally, in western blot analysis, proteins associated with cell proliferation and the G2/M checkpoint, including cyclin B1, cyclin B2, CDK1 and PCNA, were reduced in cells treated with TBZ. Protein levels were all reduced by

JPET Fast Forward. Published on November 8, 2021 as DOI: 10.1124/jpet.121.000852
This article has not been copyedited and formatted. The final version may differ from this version.

more than 60% in 300 μM TBZ (Figure 1F). These results demonstrated that levels of key checkpoint proteins paralleled cell cycle arrest induced by TBZ in GBM cell lines.

Thiabendazole inhibits invasion of GBM cells

To determine whether TBZ might inhibit infiltration capabilities of GBM cells, we examined GBM cells under TBZ treatment in trans-well and Matrigel assays. In trans-well assays, the number of P3 cells penetrating the membrane was reduced from > 250 (0 μM TBZ) to ~ 130 (150μM TBZ) and to no more than 60 (300 μM TBZ). The number of invasive U251 cells was reduced from ~ 250 (0 μM TBZ) to ~ 100 (150 μM TBZ) and ~ 35 (300 μM TBZ). After 48 h of TBZ treatment, the number of cells in both cell lines were reduced in a dose-dependent manner relative to controls (0 μM; Figure 2A). We also measured the invasive ability of GBM spheroids derived from P3 and U251 cells in suspension culture. The invasive areas of P3 spheres in Matrigel were also decreased to 65% (150 μM TBZ) and 27% (300 μM TBZ), and the invasive areas of U251 were decreased to 35% (150 μM TBZ) and 17% (300 μM TBZ) after exposure to TBZ relative to controls (0 μM TBZ; Figure 2B). Increasing TBZ concentrations furthermore led to reduced invasion (Figure 2B). In western blots performed on lysates prepared from P3 and U251 cells treated with TBZ, invasion-related proteins associated with EMT, such as N-cadherin, ZEB1 and MMP2, were downregulated > 30% with 150 μM TBZ and > 50% with 300 μM TBZ. Protein levels decreased in response to TBZ in a dose-dependent manner (Figure 2C). These results indicated that TBZ suppressed invasion of GBM cells and inhibited expression of proteins involved in EMT.

MCM2 is significantly downregulated in TBZ-treated glioma cells

JPET Fast Forward. Published on November 8, 2021 as DOI: 10.1124/jpet.121.000852
This article has not been copyedited and formatted. The final version may differ from this version.

To identify potential gene targets of TBZ, we performed RNA sequencing on RNA isolated from GBM cells treated with the molecule. GO and KEGG analysis of the resultant differentially expressed genes showed that TBZ treatment altered expression of genes associated with the cell cycle, mitosis and DNA replication (Figure 3A and 3B). Through protein-protein interaction enrichment analysis, we selected out a protein-protein interaction network involving genes regulating the G2/M phase of the cell cycle (Figure 3C and 3D). Of the top 10 differentially expressed genes in both P3 and U251 cell lines, *MCM2*, *UHRF1*, and *MCM5* showed the greatest difference in expression levels between treated and untreated cells (Figure 3E). However, we found only MCM2 to be significantly downregulated also at the protein level in both TBZ-treated P3 and U251 cell lines (Supp. Fig. 2). Moreover, MCM2 protein levels decreased in a dose-dependent manner (Figure 3F).

In Kaplan-Meier analysis performed with expression data from the TCGA and CGGA datasets, we found *MCM2* to be increased in GBM and low-grade gliomas. Furthermore, high expression of *MCM2* was related to poor survival of glioma patients (Figure 3G and 3H). These results indicate that TBZ plays a role in causing G2/M cell cycle arrest in GBM cells which is possibly mediated through the downregulation of MCM2. Thus, MCM might be a novel therapeutic target for the treatment of human glioma.

Knockdown of MCM2 inhibits glioma cell proliferation and invasion

To determine whether loss of the putative TBZ target MCM2 suppressed GBM proliferation, we used siRNA to knockdown MCM2 in P3 and U251 cells. In

JPET Fast Forward. Published on November 8, 2021 as DOI: 10.1124/jpet.121.000852
This article has not been copyedited and formatted. The final version may differ from this version.

transfection experiments performed with three small-interfering MCM2 RNAs (si-RNA 799, si-RNA 1211, and si-RNA 1355), we found two siRNAs, si-RNA 799 and si-RNA 1355, to significantly reduce MCM2 protein levels in both cell lines (Figure 4A). Cell viablity was significantly reduced in si-RNA 1355 tranfected P3 and si-RNA 799 transfected U251 after 48 h (Figure 4B). Examination of the cell cycle showed that MCM2 siRNA transfection led to an increase of cells in G2/M (11% of P3 and 14% of U251; Figures 4C and 4D). Loss of MCM2 also reduced invasion (44% for P3; 65% for U251) and migration (75% for P3; 60% for U251) of P3 and U251 cells as assessed in 3D invasion and trans-well assays (Figure 4E, 4F and Supp. Fig. 3). This reduced invasion and migration was associated with decreased expression of invasion-related proteins, N-cadherin (45% for P3; 37% for U251), ZEB1 (20% for P3; 37% for U251) and MMP2 (18% for P3; 28% for U251) in si-RNA transfected P3 and U251 cells (Figure 4G). Collectively, these data suggest that knockdown of MCM2 inhibits proliferation and invasion of GBM cells *in vitro*.

Overexpression of MCM2 reverses TBZ induced suppression of GBM cell proliferation and invasion

To determine whether increased MCM2 expression interfered with TBZ induced growth arrest in GBM cells, we created stably expressing cells through infection with lentiviral constructs expressing MCM2. P3- and U251-MCM2-OE cells showed enhanced proliferation relative to uninfected or TBZ-treated cells (Figure 5A). Overexpression of MCM2 led to a reduced percentage of cells (Negative control; MCM2 overexpression, MCM2 OE; TBZ 300 μM; TBZ 300 μM + MCM2 OE) in

JPET Fast Forward. Published on November 8, 2021 as DOI: 10.1124/jpet.121.000852
This article has not been copyedited and formatted. The final version may differ from this version.

G2/M under TBZ treatment (1.5% for U251 and 2.2% for P3, Negative control vs. MCM2 OE; 3% for U251 and 34% for P3, TBZ 300 μM vs. TBZ 300 μM + MCM2 OE) (Figure 5B and Supp. Fig. 4). Moreover, proteins associated with cell proliferation and the G2/M checkpoint, including PCNA (10% for U251 and 45% for P3, Negative control vs. MCM2 OE; 78% for U251 and 208% for P3, TBZ 300 μM vs. TBZ 300 μM + MCM2 OE), cyclin B1 (50% for U251 and 26% for P3, Negative control vs. MCM2 OE; 52% for U251, and 71% for P3, TBZ 300 μM vs. TBZ 300 μM + MCM2 OE), cyclin B2 (27% for U251 and 31% for P3, Negative control vs. MCM2 OE; 63% for U251 and 73% for P3, TBZ 300 μM vs. TBZ 300 μM + MCM2 OE), and CDK1 (147% for U251 and 62% for P3, Negative control vs. MCM2 OE; 133% for U251 and 212% for P3, TBZ 300 μM vs. TBZ 300 μM + MCM2 OE), were increased in U251- and P3-MCM2-OE cells (Figure 5C). Thus, overexpression of MCM2 rescued U251 and P3 cells from the TBZ induced G2/M arrest. Finally, in 3D invasion and trans-well assays, U251- and P3-MCM2-OE cells showed enhanced invasion (34% for U251 and 30% for P3, Negative control vs. MCM2 OE; 171% for U251, 88% for P3, TBZ 300 μM vs. TBZ 300 μM + MCM2 OE) and migration (29% for U251 and 23% for P3, Negative control vs. MCM2 OE; 206% for U251 and 163% for P3, TBZ 300 μM vs. TBZ 300 μM + MCM2 OE) in the presence of TBZ (Figure 5D and Supp. Fig. 5). Invasion-related proteins, N-cadherin (89% for U251 and 66% for P3, Negative control vs. MCM2 OE; 174% for U251 and 129% for P3, TBZ 300 μM vs. TBZ 300 μM + MCM2 OE), ZEB1 (68% for U251 and 49% for P3, Negative control vs. MCM2 OE; 21% for U251 and110% for P3, TBZ 300 μM vs. TBZ 300 μM + MCM2 OE), and MMP2 (26%

JPET Fast Forward. Published on November 8, 2021 as DOI: 10.1124/jpet.121.000852
This article has not been copyedited and formatted. The final version may differ from this version.

for U251 and 26% forP3, Negative control vs MCM2 OE; 21% for U251 and 15% for P3, TBZ 300 μM vs. TBZ 300 μM + MCM2 OE), were furthermore upregulated in U251- and P3-MCM2-OE cells (Figure 5E). In conclusion, these results indicated that overexpression of MCM2 reversed TBZ induced inhibition of proliferation and invasion in GBM cells.

TBZ inhibits growth of GBM cells *in vivo*

To examine whether TBZ inhibits GBM cell growth *in vivo*, we assessed its effects in an GBM tumor model derived from P3-luciferase expressing cells intracranially implanted in nude mice. Tumor growth was monitored using luciferase bioluminescence. TBZ treatment significantly inhibited tumor growth compared to vehicle control in the mice (Figures 6A and 6B), and the weight of TBZ-treated mice also did not decrease as rapidly relative to controls at the 2- and 3-week time points after treatment (Figure 6C). The day of death of control mice (DMSO) were the following: day 32, 35, 39, 39, and 41. The day of death of TBZ-treated mice were the following: day 39, 43, 44, 48, and 55. overall survival between control and TBZ-treated animals Kaplan-Meier analysis of the survival data also demonstrated a statistically significant difference for (median survival time 39 days vs. 44 days, controls vs. treated animals; Figure 6D). Immunohistochemistry performed on tissue sections from xenografts demonstrated that Ki67, a marker of cell proliferation, was decreased by ~ 50% in TBZ-treated tumors compared to untreated controls (Figure 6E). In addition, the expression of MCM2 was significantly decreased in xenografts from TBZ-treated mice relative to controls. Thus, TBZ inhibited tumor cell growth *in vivo*, possibly

JPET Fast Forward. Published on November 8, 2021 as DOI: 10.1124/jpet.121.000852
This article has not been copyedited and formatted. The final version may differ from this version.

through the suppression of MCM2 expression. We also examined the TBZ distribution in the brain tissue of nude mice by the liquid chromatography-tandem mass spectrometry assay. We found that the TBZ-treated sample had a transition of m/z 174.53-175.53 for an ion peak at 2.69 min (Supp. Fig. 6). This value was consistent with that of the TBZ standard solution, confirming that TBZ is capable of delivery into the tumor area in the brain.

Discussion

Benzimidazole carbamate derivatives are approved compounds for the treatment of parasitic diseases in humans. Such compounds include mebendazole, albendazole, fenbendazole, thiabendazole and flubendazole. They kill worms by binding and inhibiting beta-tubulin (Cumino et al., 2009). TBZ was FDA approved in 1967 for use in humans and has been used as antifungal treatment for a half century. Previous reports indicated that TBZ has anti-tumor effects in melanoma and fibrosarcoma, including inhibition of proliferation and migration in melanoma B16F10 cells and angiogenesis in fibrosarcoma (Zhang et al., 2013)[2]. These potential antineoplastic properties render TBZ to be of possible value as a repurposed drug for the treatment of GBM. In this study, we demonstrated that TBZ inhibited cell viability of several GBM cell lines, including P3, U251, LN229, and U118MG. The molecule suppressed proliferation of GBM cells (P3 and U251) by inducing G2/M arrest. Moreover, TBZ reduced invasion and migration of GBM cells.

Loss of cell cycle checkpoint control underlies the aggressive proliferation and dysregulation of the cell cycle associated with GBM. Thus, therapies have been designed to inhibit the cell cycle (Dominguez-Brauer et al., 2015). The mechanism of action of many microtubule inhibitors involves inhibition of the G2/M phase (Castro-Gamero et al., 2018). These drugs may be synergistic with the current standard of GBM therapy (temozolomide or radiotherapy) either by facilitating DNA damage or sensitizing malignant cells to standard therapy (Vitovcova et al., 2020). In future studies, we plan to explore the effect of the combination treatment of TBZ, TMZ and

radiotherapy on GBM.

RNA sequencing revealed potential targets of TBZ in GBM cells. Using GO, KEGG and protein-protein interaction network analysis, we found that TBZ regulates the expression of proteins that function in cell proliferation and the cell cycle. MCM2 was among the most highly differentially expressed genes under TBZ treatment, and overexpression of the gene rescued TBZ-treated cells from inhibition of cell growth. As the cytotoxic effect of TBZ (> IC50) was lower in NHA than in GBM cells, the molecule might be selective for tumor cells at certain concentrations in the clinical management of patients.

The function of MCM is regulated at elongation and termination of DNA replication (Brewster and Chen, 2010; Li et al., 2015; Seo and Kang, 2018). In the process of carcinogenesis, the dysfunction of MCM generates instability in the structure of the DNA fork, thus creating conditions for the acquisition of the gene mutations driving tumor development. As a member of the MCM family, MCM2 has been shown to be overexpressed in various tumors, including hepatocellular carcinoma (Yang et al., 2018; Yang et al., 2019), pancreatic adenocarcinoma (Peng et al., 2016; Xi and Zhang, 2018), lung cancer (Cheung et al., 2017), breast carcinoma (Yousef et al., 2017; Issac et al., 2019), ovarian cancer (Deng et al., 2019) and cervical cancer (Mukherjee et al., 2007; Amaro Filho et al., 2014). MCM2 was predicted to be a valuable prognostic biomarker in breast cancer (Liu et al., 2021), cervical cancer (Wu and Xi, 2021) and neuroendocrine prostate cancer (Hsu et al., 2021). In addition, MCM2 was suggested to be a potential treatment target to breast cancer and prostate cancer (Hsu et al., 2021;

JPET Fast Forward. Published on November 8, 2021 as DOI: 10.1124/jpet.121.000852
This article has not been copyedited and formatted. The final version may differ from this version.

Liu et al., 2021). In neuroblastoma, MCM2 expression is positively correlated with tumor growth, and thus the gene is a novel potential target for neuroblastoma pharmacological treatment (Garbati et al., 2020). Our bioinformatic analysis showed that *MCM2* is upregulated in GBM tissue (TCGA) and related to decreased survival in glioma patients (CGGA). Silencing MCM2 through siRNA knockdown inhibited proliferation and invasion of GBM cells. In contrast, the overexpression of MCM2 partially rescued GBM cells from cell cycle arrest and reduced invasion under TBZ treatment. These results suggest that MCM2 is a critical molecular target of TBZ, and warrants further study as a biomarker for TBZ as a potential treatment for GBM.

In summary, TBZ inhibits the proliferation of GBM by inducing a G2/M phase cell cycle arrest and suppresses the invasion of GBM tumor cells. TBZ downregulated the expression of MCM2, which is overexpressed in GBM based on analysis of publicly available datasets. Knockdown of MCM2 decreased GBM tumor growth and invasion *in vitro* and TBZ inhibits growth of GBM cells *in vivo*. These findings thus warrant further investigation into repurposing TBZ for the treatment of GBM patients. However, although TBZ does slow tumor growth in our animal model, eventually the tumor kills tumor bearing mice possibly due to TBZ resistant tumor cells. This recovery phase under TBZ treatment would therefore also be of interest to study in the future.

Acknowledgments

The authors thank Dr. Janice Nigro for critical comments on the manuscript.

Authorship Contributions

Participated in research design: Yaotian Hu, Wenjing Zhou, Jian Wang

Conducted experiments: Yaotian Hu, Zhiyi Xue, Xuemeng Liu, Xun Zhang, Zichao Feng, Wenjie Li and Qing Zhang

Performed data analysis: Yaotian Hu and Xiaofei Liu

Contributed to the writing of the manuscript: Yaotian Hu, Yulin Zhang, Xiaofei Liu, Wenjie Li, Qing Zhang, Anjing Chen, Bin Huang and Jian Wang

Conflict of interest

No author has an actual or perceived conflict of interest with the contents of this article.

JPET Fast Forward. Published on November 8, 2021 as DOI: 10.1124/jpet.121.000852
This article has not been copyedited and formatted. The final version may differ from this version.

References

Amaro Filho SM, Nuovo GJ, Cunha CB, Ramos Pereira Lde O, Oliveira-Silva M, Russomano F, Pires A and Nicol AF (2014) Correlation of MCM2 detection with stage and virology of cervical cancer. *Int J Biol Markers* **29**:e363-371.

Bai RY, Staedtke V, Aprhys CM, Gallia GL and Riggins GJ (2011) Antiparasitic mebendazole shows survival benefit in 2 preclinical models of glioblastoma multiforme. *Neuro Oncol* **13**:974-982.

Bell E, Jr. and Karnosh LJ (1949) Cerebral hemispherectomy; report of a case 10 years after operation. *J Neurosurg* **6**:285-293.

Brennan CW, Verhaak RG, McKenna A, Campos B, Noushmehr H, Salama SR, Zheng S, Chakravarty D, Sanborn JZ, Berman SH, Beroukhim R, Bernard B, Wu CJ, Genovese G, Shmulevich I, Barnholtz-Sloan J, Zou L, Vegesna R, Shukla SA, Ciriello G, Yung WK, Zhang W, Sougnez C, Mikkelsen T, Aldape K, Bigner DD, Van Meir EG, Prados M, Sloan A, Black KL, Eschbacher J, Finocchiaro G, Friedman W, Andrews DW, Guha A, Iacocca M, O'Neill BP, Foltz G, Myers J, Weisenberger DJ, Penny R, Kucherlapati R, Perou CM, Hayes DN, Gibbs R, Marra M, Mills GB, Lander E, Spellman P, Wilson R, Sander C, Weinstein J, Meyerson M, Gabriel S, Laird PW, Haussler D, Getz G, Chin L and Network TR (2013) The somatic genomic landscape of glioblastoma. *Cell* **155**:462-477.

Brewster AS and Chen XS (2010) Insights into the MCM functional mechanism: lessons learned from the archaeal MCM complex. *Crit Rev Biochem Mol Biol* **45**:243-256.

Campbell WC and Cuckler AC (1969) Thiabendazole in the treatment and control of parasitic infections in man. *Tex Rep Biol Med* **27**:Suppl 2:665+.

Castro-Gamero AM, Pezuk JA, Brassesco MS and Tone LG (2018) G2/M inhibitors as pharmacotherapeutic opportunities for glioblastoma: the old, the new, and the future. *Cancer Biol Med* **15**:354-374.

Cha HJ, Byrom M, Mead PE, Ellington AD, Wallingford JB and Marcotte EM (2012) Evolutionarily repurposed networks reveal the well-known antifungal drug thiabendazole to be a novel vascular disrupting agent. *PLoS Biol* **10**:e1001379.

Cheung CHY, Hsu CL, Chen KP, Chong ST, Wu CH, Huang HC and Juan HF (2017) MCM2-regulated functional networks in lung cancer by multi-dimensional proteomic approach. *Sci Rep* **7**:13302.

Cumino AC, Elissondo MC and Denegri GM (2009) Flubendazole interferes with a wide spectrum of cell homeostatic mechanisms in Echinococcus granulosus protoscoleces. *Parasitol Int* **58**:270-277.

Darlix A, Zouaoui S, Rigau V, Bessaoud F, Figarella-Branger D, Mathieu-Daude H, Tretarre B, Bauchet F, Duffau H, Taillandier L and Bauchet L (2017) Erratum to: Epidemiology for primary brain tumors: a nationwide population-based study. *J Neurooncol* **131**:547.

Deng M, Sun J, Xie S, Zhen H, Wang Y, Zhong A, Zhang H, Lu R and Guo L (2019) Inhibition of MCM2 enhances the sensitivity of ovarian cancer cell to carboplatin. *Mol Med Rep* **20**:2258-2266.

Dominguez-Brauer C, Thu KL, Mason JM, Blaser H, Bray MR and Mak TW (2015) Targeting Mitosis in Cancer: Emerging Strategies. *Mol Cell* **60**:524-536.

Gallia GL, Holdhoff M, Brem H, Joshi AD, Hann CL, Bai RY, Staedtke V, Blakeley JO, Sengupta S, Jarrell TC, Wollett J, Szajna K, Helie N, Mattox AK, Ye X, Rudek MA and Riggins GJ (2021)

Mebendazole and temozolomide in patients with newly diagnosed high-grade gliomas: results of a phase 1 clinical trial. *Neurooncol Adv* **3**:vdaa154.

Garbati P, Barbieri R, Cangelosi D, Zanon C, Costa D, Eva A, Thellung S, Calderoni M, Baldini F, Tonini GP, Modesto P, Florio T and Pagano A (2020) MCM2 and Carbonic Anhydrase 9 Are Novel Potential Targets for Neuroblastoma Pharmacological Treatment. *Biomedicines* **8**.

Gosselin RE, Smith RP and Hodge HC (1984) *Clinical toxicology of commercial products*. Williams & Wilkins, Baltimore.

Hsu EC, Shen M, Aslan M, Liu S, Kumar M, Garcia-Marques F, Nguyen HM, Nolley R, Pitteri SJ, Corey E, Brooks JD and Stoyanova T (2021) MCM2-7 complex is a novel druggable target for neuroendocrine prostate cancer. *Sci Rep* **11**:13305.

Issac MSM, Yousef E, Tahir MR and Gaboury LA (2019) MCM2, MCM4, and MCM6 in Breast Cancer: Clinical Utility in Diagnosis and Prognosis. *Neoplasia* **21**:1015-1035.

Kong Y, Feng Z, Chen A, Qi Q, Han M, Wang S, Zhang Y, Zhang X, Yang N, Wang J, Huang B, Zhang Q, Xiang G, Li W, Zhang D, Wang J and Li X (2019) The Natural Flavonoid Galangin Elicits Apoptosis, Pyroptosis, and Autophagy in Glioblastoma. *Front Oncol* **9**:942.

Lee SY (2016) Temozolomide resistance in glioblastoma multiforme. *Genes Dis* **3**:198-210.

Li N, Zhai Y, Zhang Y, Li W, Yang M, Lei J, Tye BK and Gao N (2015) Structure of the eukaryotic MCM complex at 3.8 A. *Nature* **524**:186-191.

Liu X, Liu Y, Wang Q, Song S, Feng L and Shi C (2021) The Alterations and Potential Roles of MCMs in Breast Cancer. *J Oncol* **2021**:7928937.

Mukherjee G, Muralidhar B, Bafna UD, Laskey RA and Coleman N (2007) MCM immunocytochemistry as a first line cervical screening test in developing countries: a prospective cohort study in a regional cancer centre in India. *Br J Cancer* **96**:1107-1111.

Ostrom QT, Patil N, Cioffi G, Waite K, Kruchko C and Barnholtz-Sloan JS (2020) CBTRUS Statistical Report: Primary Brain and Other Central Nervous System Tumors Diagnosed in the United States in 2013-2017. *Neuro Oncol* **22**:iv1-iv96.

Peng YP, Zhu Y, Yin LD, Zhang JJ, Guo S, Fu Y, Miao Y and Wei JS (2016) The Expression and Prognostic Roles of MCMs in Pancreatic Cancer. *PLoS One* **11**:e0164150.

Seo YS and Kang YH (2018) The Human Replicative Helicase, the CMG Complex, as a Target for Anti-cancer Therapy. *Front Mol Biosci* **5**:26.

Shergalis A, Bankhead A, 3rd, Luesakul U, Muangsin N and Neamati N (2018) Current Challenges and Opportunities in Treating Glioblastoma. *Pharmacol Rev* **70**:412-445.

Stupp R, Mason WP, van den Bent MJ, Weller M, Fisher B, Taphoorn MJ, Belanger K, Brandes AA, Marosi C, Bogdahn U, Curschmann J, Janzer RC, Ludwin SK, Gorlia T, Allgeier A, Lacombe D, Cairncross JG, Eisenhauer E, Mirimanoff RO, European Organisation for R, Treatment of Cancer Brain T, Radiotherapy G and National Cancer Institute of Canada Clinical Trials G (2005) Radiotherapy plus concomitant and adjuvant temozolomide for glioblastoma. *N Engl J Med* **352**:987-996.

Vitovcova B, Skarkova V, Rudolf K and Rudolf E (2020) Biology of Glioblastoma Multiforme-Exploration of Mitotic Catastrophe as a Potential Treatment Modality. *Int J Mol Sci* **21**.

Whalen GE, Rosenberg EB, Gutman RA, Cross J, Fresh JW, Strickland T and Uylangco C (1971) Treatment of intestinal capillariasis with thiabendazole, bithionol, and bephenium. *Am J Trop Med Hyg* **20**:95-100.

Wu B and Xi S (2021) Bioinformatics analysis of the transcriptional expression of minichromosome

maintenance proteins as potential indicators of survival in patients with cervical cancer. *BMC Cancer* **21**:928.

Xi T and Zhang G (2018) Integrated analysis of tumor differentiation genes in pancreatic adenocarcinoma. *PLoS One* **13**:e0193427.

Yang J, Xie Q, Zhou H, Chang L, Wei W, Wang Y, Li H, Deng Z, Xiao Y, Wu J, Xu P and Hong X (2018) Proteomic Analysis and NIR-II Imaging of MCM2 Protein in Hepatocellular Carcinoma. *J Proteome Res* **17**:2428-2439.

Yang WX, Pan YY and You CG (2019) CDK1, CCNB1, CDC20, BUB1, MAD2L1, MCM3, BUB1B, MCM2, and RFC4 May Be Potential Therapeutic Targets for Hepatocellular Carcinoma Using Integrated Bioinformatic Analysis. *Biomed Res Int* **2019**:1245072.

Yousef EM, Furrer D, Laperriere DL, Tahir MR, Mader S, Diorio C and Gaboury LA (2017) MCM2: An alternative to Ki-67 for measuring breast cancer cell proliferation. *Mod Pathol* **30**:682-697.

Zhang J, Zhao C, Gao Y, Jiang Y, Liang H and Zhao G (2013) Thiabendazole, a well-known antifungal drug, exhibits anti-metastatic melanoma B16F10 activity via inhibiting VEGF expression and inducing apoptosis. *Pharmazie* **68**:962-968.

Footnotes

This work was supported by the Natural Science Foundation of China (81972351), the 111 Project (B20058), the Special Foundation for Taishan Scholars (tshw201502056 and tsqn201909173), the China Postdoctoral Science Foundation (2018M642666 and 2020T130371), the Jinan Science and Technology Bureau of Shandong Province (2019GXRC006), the Shandong Research Institute of Industrial Technology.

JPET Fast Forward. Published on November 8, 2021 as DOI: 10.1124/jpet.121.000852
This article has not been copyedited and formatted. The final version may differ from this version.

Figure legends

Figure 1. Thiabendazole promotes G2/M arrest in GBM cells *in vitro*. (A) CCK-8 assays to measure cell viability of P3, U251, LN229, A172, U118MG and NHA treated with TBZ at different concentrations for 48 h. Data points represent the percentage (%; OD450 treated/OD450 untreated) relative to untreated cells. (B) IC50 value of cell lines P3, U251, LN229, A172, U118MG and NHA calculated with GraphPad Prism 8. (C) CCK-8 assays to measure cell viability of P3 and U251 with TBZ at different concentrations (0 μM, 100 μM, 200 μM and 300 μM) and at different time points (24 h, 48 h, 72 h and 96 h). Data points are the OD450 values. All data are expressed as the mean ± SD of values from triplicate experiments. (D) Analysis of EdU-positive cells of P3 and U251 treated with different concentrations of TBZ for 48 h. The percentage of EdU-positive cells (EdU-positive/DAPI-positive × 100%) was quantified in 3 random fields per sample. (E) Data points represent the percentage of cells in G0/G1and G2/M in P3 and U251 at 48 h after TBZ treatment. (F) Western blot to detect levels of cyclin B1, cyclin B2, CDK1 and PCNA and β-actin in P3 and U251. All data are expressed as the mean ± SD of values from triplicate experiments. * $P < 0.05$, ** $P < 0.01$ and *** $P < 0.001$ compared to controls.

Figure 2. Thiabendazole inhibits GBM cells invasion**.** (A) Trans-well invasion assays for P3 and U251 cell lines treated with TBZ (150 μM and 300 μM) or DMSO (0 μM). Graphic representation of trans-well cell number for P3 and U251treated with TBZ (150 μM and 300 μM) or DMSO (0 μM). (B) 3D invasion assays for P3 and U251 (scale bars: 200 μm) treated with TBZ (150 μM and 300 μM) or DMSO (0 μM). Graphic representation of ratio values of the invasion area to the core area. (C) Western blot to determine expression levels of ZEB1, N-cadherin, MMP2 and β-actin (protein loading control) in P3 and U251 cells treated with DMSO or TBZ at the indicated

JPET Fast Forward. Published on November 8, 2021 as DOI: 10.1124/jpet.121.000852
This article has not been copyedited and formatted. The final version may differ from this version.

concentrations for 48 h. All data are expressed as the mean ± SD of values from triplicate experiments. * $P < 0.05$, ** $P < 0.01$ and *** $P < 0.001$ compared to controls.

Figure 3. MCM2 mRNA and protein are downregulated by thiabendazole in GBM cells *in vitro*. (A) GO analysis on the differentially expressed mRNAs identified by RNA sequencing of RNA isolated from TBZ-treated P3 and U251 cell lines vs controls. (B) Pathway enrichment analysis of the differentially expressed mRNAs identified through RNA sequencing of RNA isolated from TBZ-treated P3 and U251 cell lines compared to controls. (C) Protein-protein interaction enrichment analysis to predict genes interacting with other genes. (D) TargetScanHuman to predict the network of protein-protein interaction derived from the differentially expressed genes associated with the cell cycle. (E) Top 10 genes with greatest fold change in mRNA expression levels (fold change value > 1000) in P3 and U251, respectively. Intersecting genes, *MCM2*, *MCM5*, *UHRF1,* downregulated in P3 and U251 cells are highlighted in red. (F) Western blot to determine expression levels of MCM2 and GAPDH (protein loading control) in P3 and U251 cells treated with DMSO or TBZ at the indicated concentrations for 48 h. (G) Analysis of expression levels of *MCM2* mRNA in normal brain tissue samples (NBT) and GBM samples in the publicly available database TCGA. *$P < 0.05$. (H) Kaplan-Meier analyses to determine differences in overall survival for patients with low and high *MCM2* expressing primary gliomas. High MCM2 expression group expresses more MCM2 than median expression, while low MCM2 expression group expresses less MCM2 than median expression. The data were obtained from the CGGA database.

Figure 4. Knockdown of MCM2 inhibits GBM cell proliferation and invasion. (A) Western blot to assess knockdown efficiency of MCM2 by siRNA in P3 and U251 cells. (B) CCK-8 assays to measure cell viability of P3 and U251 transfected with MCM2 and control si-RNAs. Data points

JPET Fast Forward. Published on November 8, 2021 as DOI: 10.1124/jpet.121.000852
This article has not been copyedited and formatted. The final version may differ from this version.

are OD450 values. $^{**}P < 0.01$, $^{***}P < 0.001$. (C) Cell cycle distribution of P3 and U251 determined with PI staining by flow cytometry analysis. Data points are the percentage of cells in G0/G1and G2/M in P3 and U251 at 48 h after si-RNA transfection. (D) Western blot to detect expression levels of cyclin B1, cyclin B2, CDK1 and GAPDH (protein loading control) in P3 and U251 cells 48 h after si-RNA transfection. (E) 3D invasion assays for P3 and U251 transfected with MCM2 or control si-RNA (scale bars: 200 μm). Graphic representation of the ratio values of the invasion area to the core area. $^{**}P < 0.01$. (F) Quantification of trans-well cell number for P3 and U251cells transfected with MCM2 or control si-RNA. ** $P < 0.01$, $^{***}P < 0.001$. (G) Western blot to determine expression levels of N-cadherin, ZEB1, MMP2 and GAPDH in P3 and U251 transfected with MCM2 or control siRNA.

Figure 5. Overexpression of MCM2 rescues GBM cells from TBZ inhibition. (A) CCK-8 assays to measure cell viability of P3- and U251-MCM2-OE and parental cell lines under the conditions indicated. (B) The percentage of cells in G2/M in the four treatment groups. (C) Western blot to determine expression levels of MCM2, cyclin B1, cyclin B2, CDK1 and GAPDH in P3- and U251-MCM2-OE and parental cell lines under the conditions indicated. (D) 3D invasion assays for P3- and U251-MCM2-OE and parental cell lines under the conditions indicated (scale bars: 200 μm). Graphic representation of ratio values of the invasion area to the core area. (E) Western blot to detect expression levels of N-cadherin, ZEB1, MMP2 and GAPDH in P3- and U251-MCM2-OE and parental cell lines under the conditions indicated. All data are expressed as the mean ± SD of values from triplicate experiments. ns = none-significant, $^{*}P < 0.05$, $^{**}P < 0.01$ and $^{***}P < 0.001$.

Figure 6. TBZ inhibits tumor growth in an orthotopic model for GBM in mice. (A) P3-luciferase cells were orthotopically implanted into nude mice, and tumor growth was followed by

JPET Fast Forward. Published on November 8, 2021 as DOI: 10.1124/jpet.121.000852
This article has not been copyedited and formatted. The final version may differ from this version.

the detection of bioluminescent signals under the PerkinElmer IVIS Spectrum at days 7, 14, and 21 after implantation. (B) Quantification of bioluminescence values to determine tumor growth at days 7, 14, and 21. (C) Quantification of the weight of nude mice in each experimental group at days 0, 7, 14, 21 and 28. (D) Kaplan-Meier analysis to determine overall survival of tumor bearing nude mice and log-rank test to assess the statistical significance of the differences. (E) Immunohistochemistry staining for Ki67 and MCM2 in the tumor sections of nude mice from each group as indicated (scale bars: 100 μm). Graphic representation of the percentage of Ki-67 and MCM2 positive cells in the tumor sections. All data are expressed as the mean ± SD of values from triplicate samples. $*P < 0.05$, $**P < 0.01$, $***P < 0.001$ compared between the 2 treatments.

JPET Fast Forward. Published on November 8, 2021 as DOI: 10.1124/jpet.121.000852
This article has not been copyedited and formatted. The final version may differ from this version.

Figure 1

A

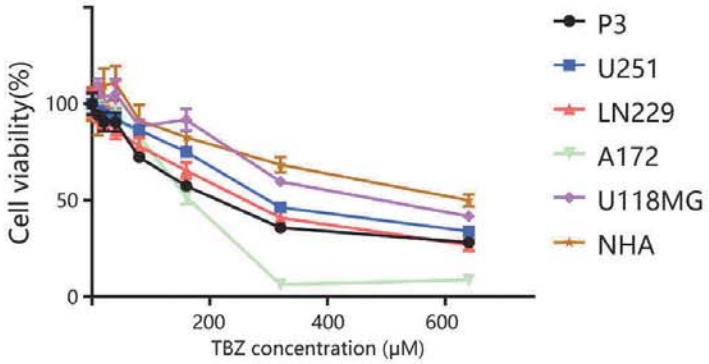

B

Cell Line	Ic50 (μM)
P3	215.1
U251	346.0
LN229	266.0
A172	160.4
U118MG	455.5
NHA	561.0

C

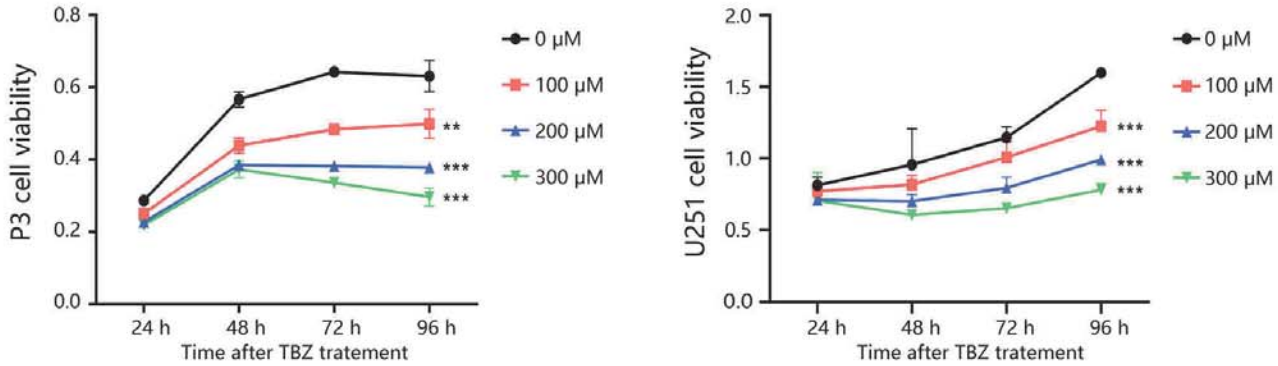

D

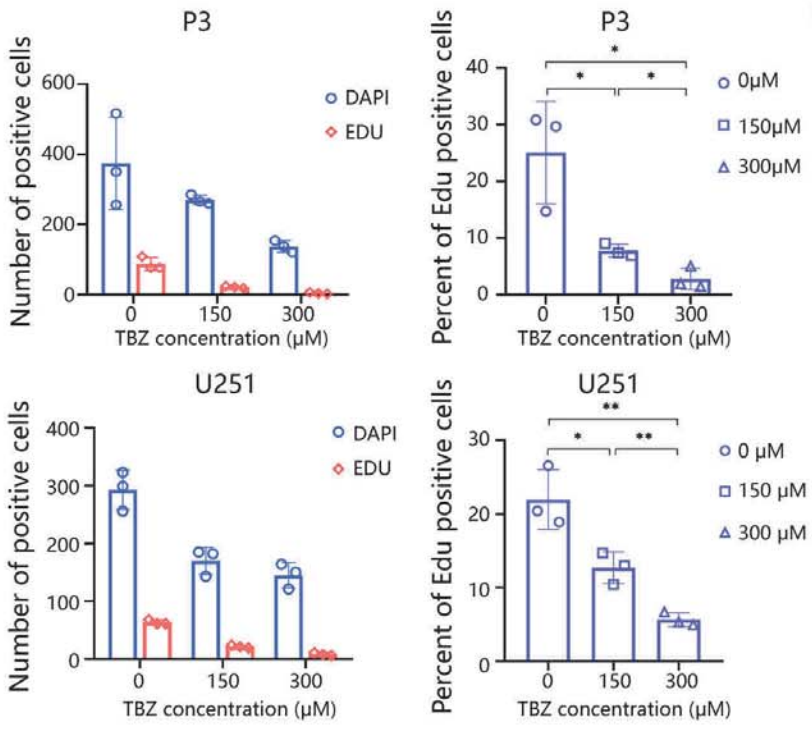

E

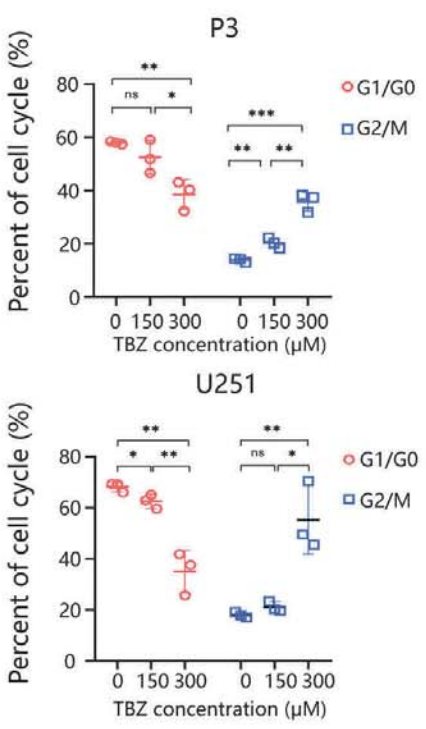

F

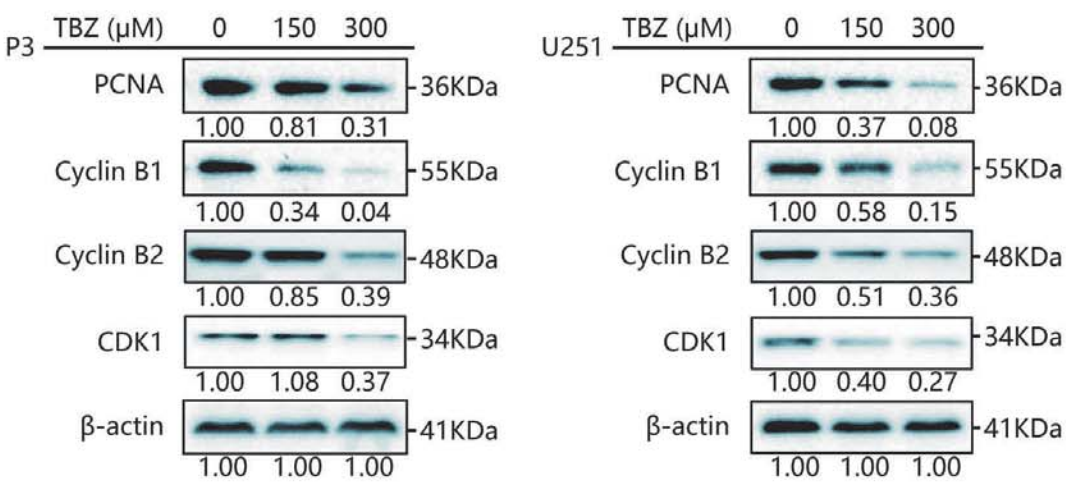

JPET Fast Forward. Published on November 8, 2021 as DOI: 10.1124/jpet.121.000852
This article has not been copyedited and formatted. The final version may differ from this version.

Figure 2

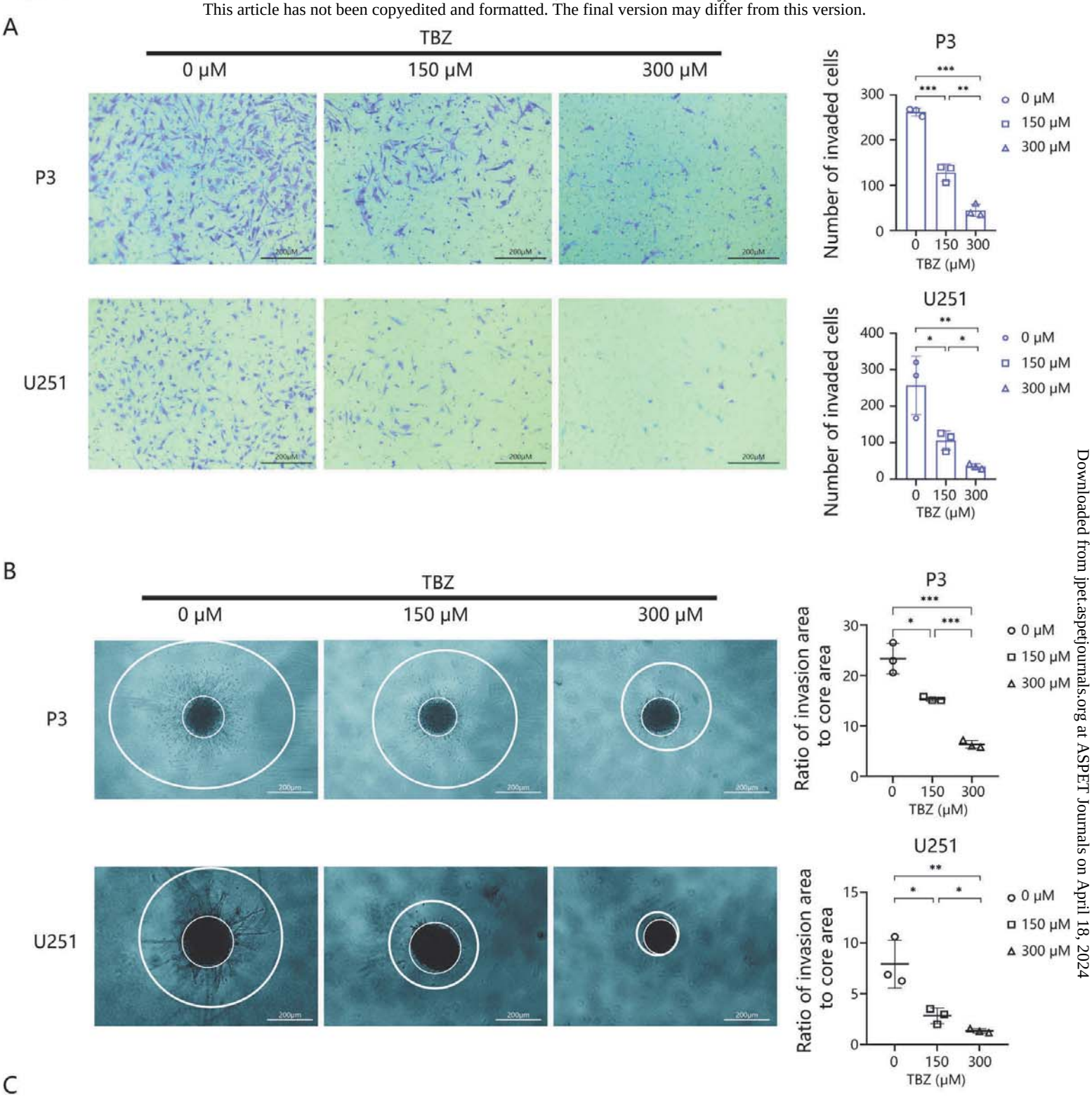

JPET Fast Forward. Published on November 8, 2021 as DOI: 10.1124/jpet.121.000852
This article has not been copyedited and formatted. The final version may differ from this version.

Figure 3

A

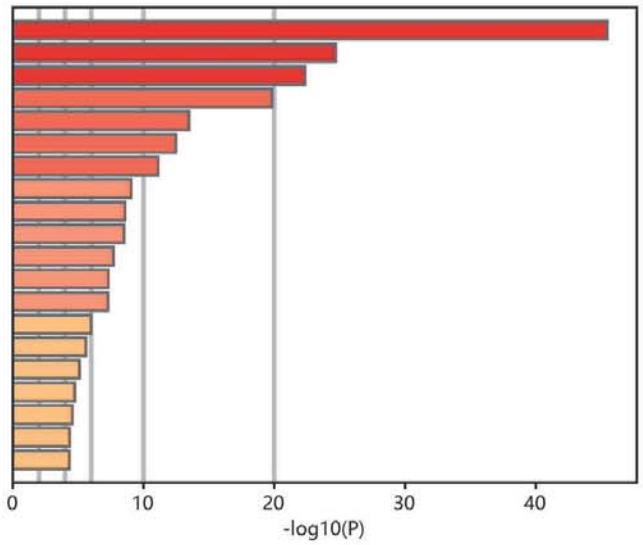

R-HSA-69278: Cell Cycle, Mitotic
GO:0007059: chromosome segregation
R-HSA-69620: Cell Cycle Checkpoints
GO:0071103: DNA conformation change
GO:0007017: microtubule-based process
R-HSA-2299718: Condensation of Prophase Chromosomes
M129: PID PLK1 PATHWAY
M14: PID AURORA B PATHWAY
GO:1903046: meiotic cell cycle process
R-HSA-983231: Factors involved in megakaryocyte development and platelet production
GO:0000281: mitotic cytokinesis
GO:0010639: negative regulation of organelle organization
GO:0090068: positive regulation of cell cycle process
GO:0007062: sister chromatid cohesion
R-HSA-380320: Recruitment of NuMA to mitotic centrosomes
M46: PID ATR PATHWAY
CORUM:7542: KNL1-MIS12-NDC80-SPC24-ZWINT complex
CORUM:1108: DNA synthesome complex (15 subunits)
GO:0051640: organelle localization
GO:0000076: DNA replication checkpoint

B

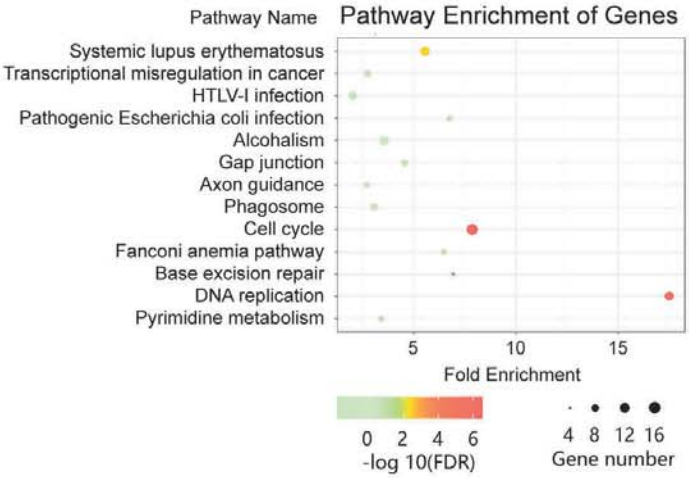

C

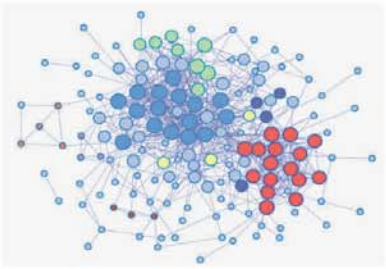

Color	MCODE	Go	Description	Log10(P)
	MCODE1	R-HSA-141424	Amplification of signal from the kinetochores	-35.4
	MCODE1	R-HSA-141444	Amplification of signal from unattached kinetochores via a MAD2 inhibitory signal	-35.4
	MCODE1	R-HSA-69618	Mitotic Spindle Checkpoint	-34.3
	MCODE2	R-HSA-69278	Cell Cycle, Mitotic	-23.5
	MCODE2	R-HSA-1640170	Cell Cycle	-22.3
	MCODE2	R-HSA-69481	G2/M Checkpoints	-15.5
	MCODE3	GO:0006260	DNA replication	-15.7
	MCODE3	GO:0006261	DNA-dependent DNA replication	-14.6
	MCODE3	R-HSA-176187	Activation of ATR in response to replication stress	-12.5

D

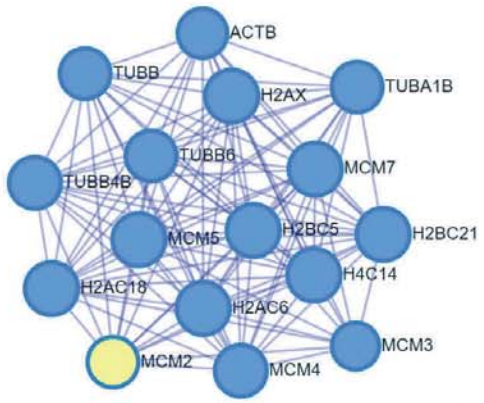

E

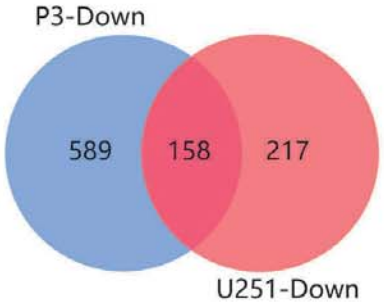

mRNA expression log2 fold change top10
(mRNA expersion >1000)

P3	U251
RRM2	UHRF1
DTL	TUBA1B
MCM5	MCM2
UHRF1	IQGAP3
MCM4	KPNA2
ESPL1	TUBB
ZWINT	ASPM
FANCI	MCM5
MCM2	MCM6
KNTC1	FAM83D

F

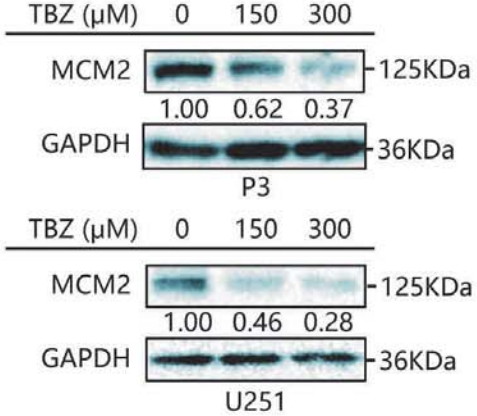

G

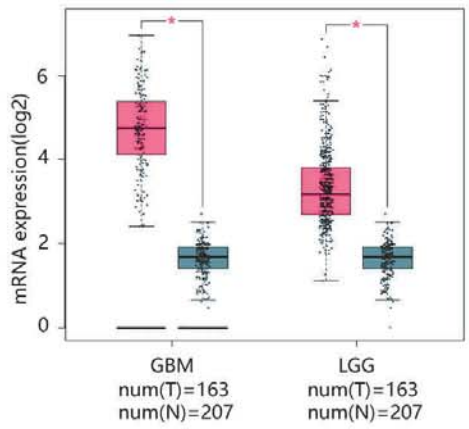

H

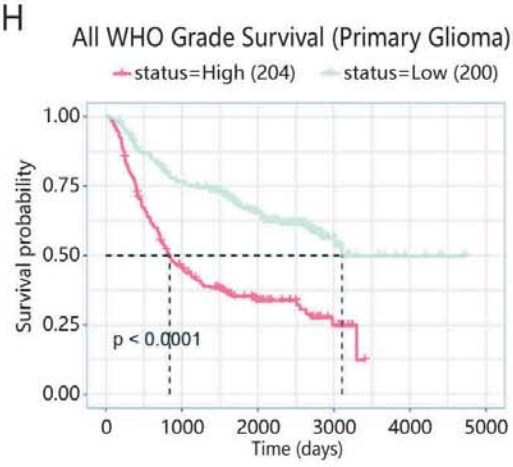

JPET Fast Forward. Published on November 8, 2021 as DOI: 10.1124/jpet.121.000852
This article has not been copyedited and formatted. The final version may differ from this version.

Figure 4

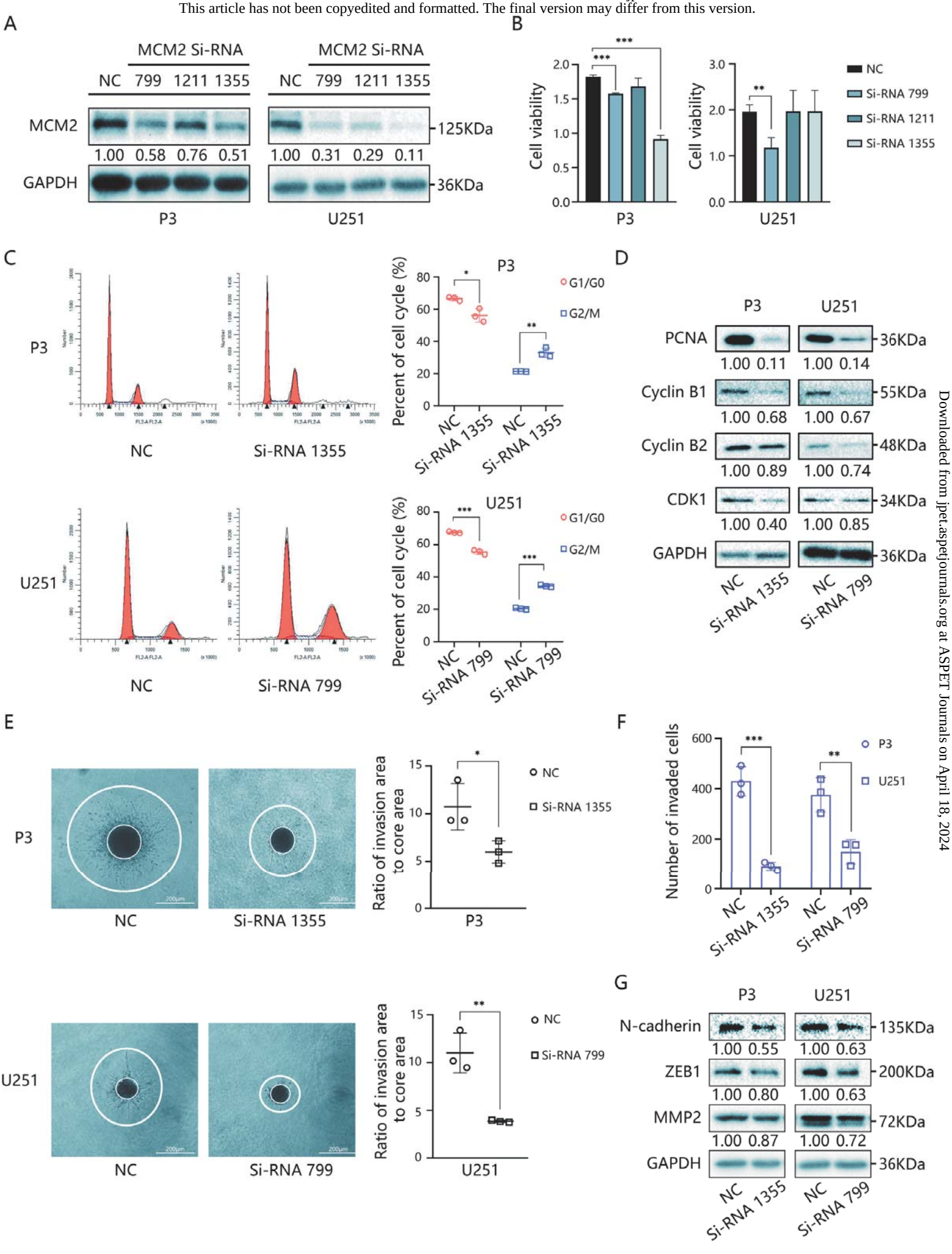

JPET Fast Forward. Published on November 8, 2021 as DOI: 10.1124/jpet.121.000852
This article has not been copyedited and formatted. The final version may differ from this version.

Figure 5

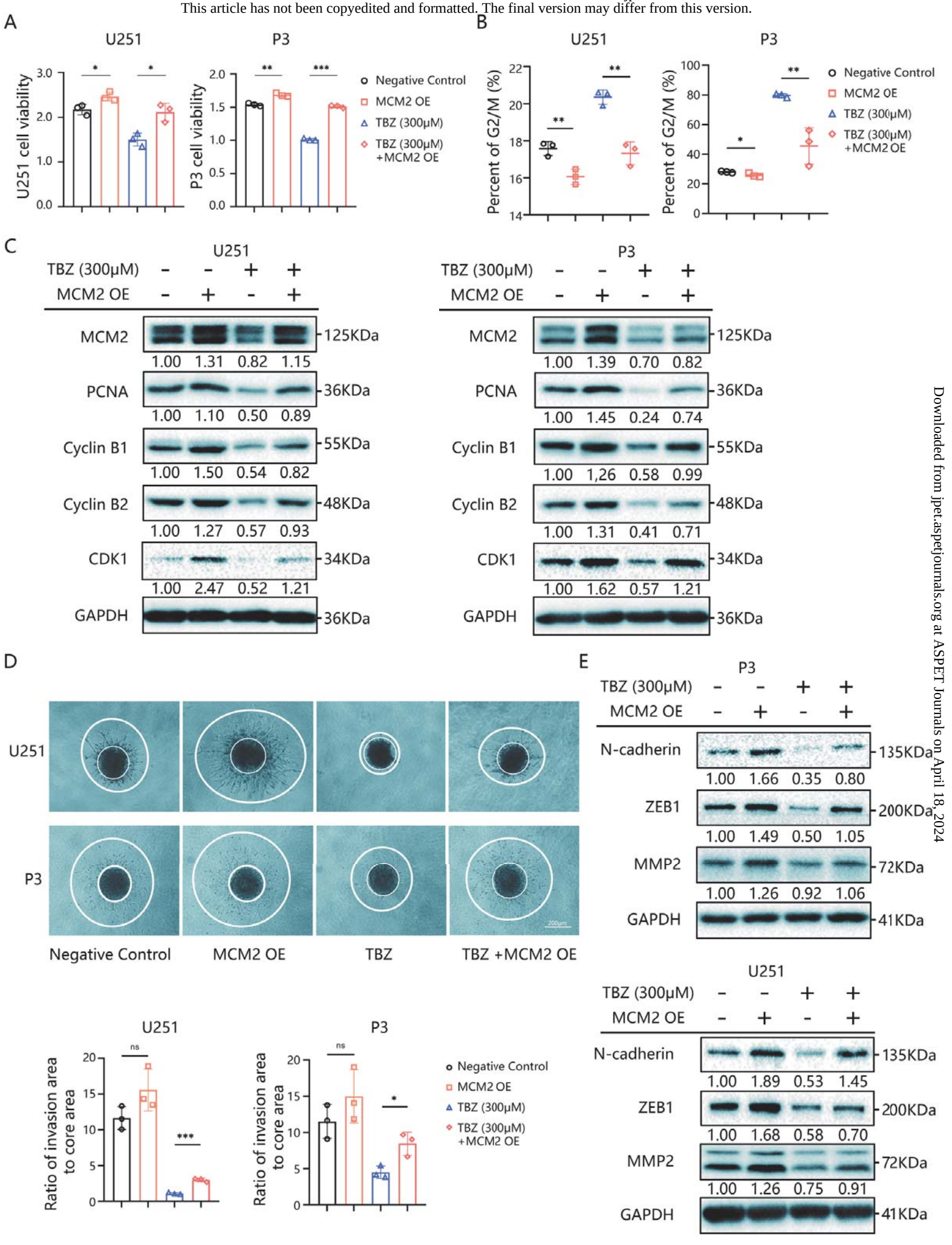

JPET Fast Forward. Published on November 8, 2021 as DOI: 10.1124/jpet.121.000852
This article has not been copyedited and formatted. The final version may differ from this version.

Figure 6